NUMERICAL MODELING OF CLEAR WATER BORE IMPACT

ENRICO BERTOLAZZI[1] AND FILIPPO TRIVELLATO [2]

[1] *Department of Mechanical and Structures Engineering, University of Trento,*
via Mesiano 77, I – 38050 Trento, Italy
Fax : +39 0461 882599 Voice : +39 0461 882590
E-mail: Enrico.Bertolazzi@ing.unitn.it

[2] *Department of Civil and Environmental Engineering, University of Trento,*
via Mesiano 77, I – 38050 Trento, Italy
Fax : +39 0461 882672 Voice : +39 0461 882631
E-mail: Filippo.Trivellato@ing.unitn.it

Abstract

The impact of a bore on a wall generates hydrodynamic pressure and overturning bending moment about the base of the wall. The knowledge of the hydrodynamic loading is crucial in the rational design of protection structures. The aim of the present work is to present a finite volume element method, combined with a Runge-Kutta scheme for time step advancing, that is capable of calculating the highly unsteady, incompressible, free surface flow field due to the collision of a clear water bore on a vertical plane wall. The bore is assumed to be generated as a dam-break wave and to propagate along a dry bed. The impact phenomenon is modelled in two dimensions by a fully nonlinear potential approach. A discrete formulation is implemented to trace accurately the pathline of the nodes on the free surface. The experimental physical data were observed to have a poor repeatability in spite of sharing the same initial conditions. The fact that realistic initial conditions are missing did not allow a full comparison between the numerical solution and the experimental data; other likely sources of discrepancies are also discussed. The present numerical approach proved successfull in obtaining a quantitative evaluation of the physical quantities that are of interest for civil engineers such as the maximum force acting on the wall. Air entrainment in the bore is well developed; however, it is suggested that the thrust of the bore is not remarkably changed by air entrainment as long as mean air concentration in the toe is less than 0.3.

Keywords. bore, impact, non linear, free surface, Runge-Kutta.

NOTATION

C	Mean air concentration $(/)$;
h_f	Bore depth at the impact time (L);
K	Total number of nodes $(/)$;
L_o	Distance of influence (L);
M	Clear water bore momentum flux (ML/T^2);
M_m	Air–water bore momentum flux (ML/T^2);
N	Number of nodes on the free surface $(/)$;
Q	Volumetric flowrate (L^3/T);
$\mathbf{S} = (S_1, S_2)$	Parametric form of the free streamline (L);
t	Temporal variable (T);
T_r	Rise time (T);
u	Horizontal component of velocity (L/T);
u_o	Velocity of the bore toe near the test wall (L/T);
v	Vertical component of velocity (L/T);
$\mathbf{V} = (u, v)$	Velocity vector (L/T);
x	Horizontal co–ordinate (along the flume) (L);
$\mathbf{x} = (x, y)$	Coordinate vector (L);
y	Vertical co–ordinate (along the wall) (L);
Γ_s	Free surface boundary (L);
Γ_w	Impermeable wall boundary (L);
θ	Free surface parametric coordinate $(/)$;
ρ	Liquid mass density (M/L^3);
ϕ	Potential function along the free surface (L^2/T);
Φ	Potential function (L^2/T);
$\Omega(t)$	Time–dependent liquid computational domain (L^2).

1. Introduction

The phenomenon of the collision of a fluid mass with an obstacle has received much attention in the literature not only for its social relevance, but also because it is of interest to scientists involved in different research topics. Examples are sea–waves or tsunamis impacting on breakwaters, hydrodynamic pressure on dams due to seismic waves, formation of glassy metals by a fluid jet and heat transfer from a jet fluid to a surface. A new topic should be nowadays included in the above list, the impact of mud and debris–flows on check–dams.

An exhaustive review of structures conceived to control the propagation of debris–flows is reported by Okubo et al. [1997]. Due to inertial effects, debris–flow collision does generate dynamic pressure on structures together with the associated overturning bending moment about the structure's base. The knowledge of the dynamic loading is crucial in the rational design of these transversal structures.

While hydraulic design of such a structures can be verified with reasonable accuracy by physical modeling [Armanini and Trivellato, 1990], structural design related to dynamic loading is still founded mostly upon both past experience and field observations.

The motivation of this work is twofold: on the one hand, it is believed that the complex dynamics of the impact phenomenon can be described by a simple analytical approach. On the other hand, it is desiderable to obtain wall force predictions that are useful to the practicing engineer to carry out a rational design of protection structures.

The description of the physical phenomenon is presented in par. 2 while the analytical problem is formulated in par. 3. Details about the implementation of the numerical scheme are described in par. 4; results are presented in par. 5, which is followed by a discussion and the relevant conclusions.

1.1. Literature review

The problem of a liquid mass colliding with a solid body is a broad subject which includes relevant parts of fluid mechanics. Interest in this topic arose in the early decades of this

century – see, for instance, the review by Korobkin and Pukhnachov [1988]. The impact of a steady fluid jet has been studied in depth by many authors under more general hypotheses: a review is found in Weber and Hureau [1999]. For a comprehensive review of the literature concerning wave impact pressures, impact of water drops and the water entry of a solid wedge, see Cooker and Peregrine [1995]. The impingement of steady circular jets has been thoroughly studied by Beltaos and Rajaratnam [1974]. The steady impact of a water wedge which is assumed of infinite extent has been formulated in terms of similarity variables [Cumberbatch, 1960]. The problem of determining the free surface of a two dimensional jet of an ideal fluid has been solved by Peng and Parker [1997], while the evaluation of wall shear stress, involving also compressibility effects, has been tackled by Phares et al. [2000]. The above theories apply to steady state conditions.

As for unsteady collisions, the review of the literature does not give much assistance in collecting useful informations to assess the dynamic loading experienced by a wall due to the collision of a bore propagating on a dry bed, apart from the laboratory physical experiments performed by Scotton [1996], which will be briefly described in par. 2, and the theoretical approach proposed by Armanini and Scotton [1993] in case of debris–flow collision.

One possibility for a theoretical approach was prompted by the resemblance that can be conjectured between bore collision and hydrodynamic pressure on dams due to a horizontal seismic movement. Considering a vertical rigid surface, Westergaard [1933] stated that the maximum pressure occurs at the dam base, its maximum value being $0.742\rho a h_f$ (where ρ is the water mass density, a is the horizontal seismic acceleration, h_f the depth of the liquid bath), a result confirmed by means of the pressure–impulse theory [Cooker and Peregrine, 1995]. As a first approximation, the pressure due to the bore collision was conceived to be due basically to the displacement experienced by the structure in the first quarter of the period of a fictitious sinusoidal earthquake [Scotton and Trivellato, 1995b], the interest being in fact only in predicting the maximum value of the dynamic pressure and not in studying the whole temporal evolution of the wall pressure. According to the seismic model, the

relevant scales are: the temporal scale T_r (the rise time, i.e. the time the maximum deceleration occurs) and the length scale h_f. However, h_f was demonstrated not to be the proper length scale and was instead redefined as the maximum run–up height of the jet after the impact [Scotton and Trivellato, 1995a]. A better interpretation of the experimental data was then obtained (incidentally, the effects of a typical debris–flow collision could be roughly compared to an 11 magnitude earthquake, which is beyond the maximum value of the Richter classification).

Relevant applications of the mathematical model based on the pressure–impulse concept have been proposed by Cooker and Peregrine [1995] in case of breaking sea–waves striking a vertical rigid surface; by Korobkin and Peregrine [2000] to know the energy distribution due to the impact of a half-submerged sphere; by Wood et al. [2000] for the trapping of an air pocket and by Wood and Peregrine [2000] to account for a porous berm.

Among coastal engineers, the formula of Goda [1985] is popular in assessing wave forces on breakwaters. The experimental results of Ramsden and Raichlen [1990] are relevant to assess the force experienced by a vertical wall due to the impact of a bore generated by a broken solitary wave and propagating over a liquid bath at rest. The presence of water in the channel ahead of the surge does affect the shape of the wave tip as well as the generation of forces [Cross, 1967]. The study of the impulsive motion of a flat plate in an inviscid, compressible fluid has been carried out by Miles [1953] on the basis of the acoustic approximation.

As for the numerical solutions, fully nonlinear potential flow computations have been performed in literature using a large variety of methods for the treatment of the free surface, for a review of which see, among others, Beck [1999]. It is well known that locating the free surface is by far the most demanding task in the analysis of moving free surface flows. Numerical schemes which are helpful in solving this kind of problems are best classified as Lagrangian and Eulerian schemes. Volume of Fluid (VOF) method is also popular and it can be conveniently applied to existing numerical codes [Shin and Lee, 2000]. A numerical study of the 2–D impact of a plunging wave on a rigid vertical wall, in the contest of

potential flow, has been performed by Zhang et al. [1996], who considered also the effect of an air cushion trapped in between the plunger and the wall. Among the most accurate boundary integral numerical methods, the one developed by Dold and Peregrine [1986] is based on the Cauchy's integral. Mohapatra et al. [2000] solved the Euler's equations for the impact of a bore propagating over a static liquid bath.

The literature devoted to the many occurrences of the impact phenomenon is large; the above review shows that exaustive results on water impact have been collected, but none in the case of a bore generated by a dam–break and propagating along a dry–bed. Further the phenomenon of air entrainment in the bore rushing downstream has not been addressed. This last effect can be significant in determing the bore thrust and in jeopardizing the reliability of the extrapolation of the experimental results from the model scale to the prototype scale.

2. Description of the phenomenon

Physical experiments were conducted at the Hydraulic Laboratory of the University of Trento (Italy). The experimental tests were originally intended to simulate debris–flow collisions on walls. The description of the experimental apparatus and of the comprehensive experimental database are detailed in Scotton [1996] and in Trivellato and Scotton [2001]. The experimental apparatus comprised a 6 meter long tilting flume. Flume slopes varied from 0° through 25°. The flume cross–section was 0.5 m wide and 0.5 m deep. In the upstream part of the flume, a feeding box was arranged where either clear water or a mixture of granular material and water could be accommodated. The mixture was released into the flume by an impulsively opened flap–gate to generate a bore. Then the bore advanced in a dry bed. The downstream part of the flume was made of a transverse wall that was suitably instrumented with four gauges to measure impact pressures. The diameter of the *flush–to–the–wall* pressure membrane was 1 cm. A frequency response of 250 Hz turned out to be convenient in recording the unsteady phenomenon. The measured pressures reached

25 kPa. In spite of the great effort dedicated in performing accurate experiments, a poor repeatability was detected in the tests: in fact, the difference in pressure intensities among experiments sharing the same initial conditions was as high as a $5\% \div 15\%$. This observation is consistent with what already claimed by a number of authors (see, for instance, Dold and Peregrine [1986], Zhang et al. [1996]). A significant scatter (which could even go as high as $\pm 50\%$) in peak pressures was documented by Kirkgöz [1982]. Poor repeatability was mostly due to the ever–changing evolution of the breaking front, the structure of which has strong 3-D patterns. As an obvious result, the modes of impact differ in each experiment. A pure 2–D impact is expected to produce higher pressures than the 3–D case. The measured duration of the impact was found to be in accordance with known values of similar phenomena, e.g., plunging waves on vertical sea–walls [Ramsden and Raichlen, 1990, Zhang et al., 1996]. Toe velocities u_o and toe depths h_f of the bore near the wall were measured by a video–recording apparatus (SVHS video–camera, 25 frames per second, shuttering time $1/1000$ s). The measurements of *unsteady* toe velocities were performed by tracing the location of the most advanced part of the ever–breaking front rushing downstream; clearly this procedure suffered from 3–D effects.

Due to the rounded geometry of the snout, any definition of the toe is not satisfactory. In the laboratory experiments, the undisturbed depth h_f of the bore near the wall at the time T_r (the time the maximum force occurs or, in other words, the time the maximum deceleration occurs) was chosen as the significant depth. The knowledge of T_r is definitely of interest; yet its measurement is neither easy nor univocal.

In the physical experiments the surge met the test wall at a normal incidence; according to Whillock [1987], waves having a slight oblique angle of impact can originate higher forces than normally incident waves.

As stated by Peregrine and Topliss [1994], the compressibility of pure water does not play a significant role in this kind of impacts. Owing to air entrainment, the velocity of sound in air–water mixtures can be even one order of magnitude less than that in pure water; even so the compressibility of the mixture is expected to be unimportant in actual

prototype collisions.

As opposed to near–breaking sea waves impacts, there is no trapping of an air pocket between the surge and the wall. At the very beginning of the collision process, the upward motion forming at the wall is of the flip–through type, according to the definition given by Peregrine and Topliss [1994]. The flip–through is the upward jet originated – in a time scale of milliseconds – by the liquid toe before the main body of the surge meets the rigid surface.

Important secondary circulations are generated at the instant of impact and massive air entrainment is observed to occur in the liquid toe before and after the impact. Due to the above phenomena, the temporal evolution of the wall pressure was observed to be pulsating. Typical features worth mentioning are:

(i) an initial sharp peak of pressure of short duration ($\sim 10^{-1}$ s) due to the toe collision. High forces are generated from such maximum pressures and a vertical jet of remarkable height is formed;

(ii) a pressure of long duration (~ 1 s), normally decaying with time, whose pulsating behavior is due both to trapped air and to small scale vortices;

(iii) a peak pressure of short duration ($\sim 10^{-1}$ s), due to the collapsing of the run–up jet down onto the incoming surge at the bottom. This final peak has been found to be less severe than the first one, as opposed to the case of tsunamis and sea bores [Cross, 1967, Ramsden and Raichlen, 1990].

The diagram of the force experienced by the wall behaves basically in the same way as the pressure evolution. The wall force was computed by integrating the pressure measurements [Trivellato and Scotton, 2001]; the force diagram displays the rise time T_r, i.e. the time the force attains its maximum. Yet in some instances – typically whenever the flume slope is horizontal – it is difficult to make the proper choice among several maxima occurring within a short period of time. So it was suggested that T_r be chosen whenever one of the maxima of the wall force is in phase with the pressure first maximum of the gauge whose elevation is nearest to the debris depth [Scotton and Trivellato, 1995a].

As already claimed by Peregrine and Topliss [1994] in case of sea waves, the measurements reported in Trivellato and Scotton [2001] confirmed that the maximum wall force does not occur at the time of maximum run-up height, the thin crest of which contributes nothing to the force at the wall. The time of the maximum run–up follows the time of the maximum force.

2.1. Air entrainment

The phenomenon of air entrainment was observed to be one of the major features occurring during the propagation of the dam–break generated physical bore. The phenomenon is readily visible by video camera frames in the ever–breaking front wave rushing downstream, which produces strong agitation in the flow. The entrained air is distributed all over the rolling front wave and it is controlled by the intensity of the turbulence present in the flow. In the front region, the air entrainment is extremely developed even for a surge propagating along a horizontal bottom. As the front region contributes the most to the evolution of the impact force at the wall, it is the most important region to consider.

In the rear region, the flow pattern is definitely more organized and most of the turbulence generated in the toe region is being dissipated, resulting in a less chaotic flow. The rear flow pattern evolves towards superficial self–aeration, i.e. air is entrained only at the free surface, with a dramatic reduction of air content as compared to the front region. Self–aeration occurs as soon as the turbulent velocity fluctuations are capable of overcoming both the surface tension pressure and the rise velocity component of the entrained bubble. Considering both of the above effects, Chanson [1993] proposed criteria for air entrainment to occur. Air entrainment is also enhanced by the turbulence that is generated while the impact is progressing. Air entrainment in the upward flowing jet is highly promoted at the wall elevation L_o, where the pressure along the wall normal is atmospheric.

Effects of air entrapment are flow bulking and the reduction of the bore density which becomes smaller than that of the pure water. Further, the presence of air within the boundary layers of the bottom and lateral walls causes a reduction of the shear stress and an

increase of momentum.

Prediction formulae of literature are available only for uniform or gradually varied flows and cannot be extended meaningfully to the present instance of unsteady motion either in the front region (air is entrapped like in a hydraulic jump or like in breaking sea-wave) or in the rear region.

It is desiderable for design purpose to have theoretical models to guide the proper scaling of the phenomenon. Since the dominant effects are taken to be those of gravity and inertia, the most obvious scaling between experiment and prototype is the Froude scaling. However, air entrainment data measured on physical models cannot be extended straightforwardly to the prototype scale if laboratory models are operated according to the Froude's law, since the air release mechanism is not properly modelled by this law, apart from further considerations regarding the reproduction of the turbulence field. In the prototype, entrained air persists both for relatively greater distances and for longer times. Scaling laws for model–prototype extrapolation are not fully reliable in case of sea–waves [Führböter, 1986], and the model–prototype extensibility of results is as yet an open problem in the case of bore impact.

The pressures measured in laboratory physical experiments should correspond to smaller values in the prototype where air entrainment is greater and the density of the air–water mixture is less than that of the pure water. Peregrine and Thais [1996] found a large reduction in pressure even for small air content.

In spite of the pressure reduction, the total force acting on the wall is likely unmodified, since air entrainment increases bulking even though it decreases the mixture density, so that the total liquid mass involved in the collision – and the total momentum likewise – is expected to be basically unchanged, at least when a steady state is attained.

The following simplified reasoning can be of help in understanding the constancy of the momentum. In case of no air entrainment, the momentum flux of the bore as it advances

along a horizontal bed is written as:

$$M = \rho Q u_o = \rho u_o^2 h_f$$

The same quantity in case of air entrainment should be intended instead as:

$$M_m = \rho_m u_o^2 h_{fm}$$

where the subscript m stands for mixture (of air–water) and where it is assumed in the first approximation that u_o is not changed by the presence of air. The depth h_{fm}, called the bulked depth, and the bulk density ρ_m are given by [Rao and Kobus, 1973]:

$$\begin{aligned} h_{fm} &= \frac{h_f}{(1-C)} \\ \rho_m &= \rho\,(1-1.1\,C), \qquad 0.2 \le C \le 0.85 \\ C &= \frac{V_a}{V_a + V_w} \end{aligned}$$

where C is the mean air concentration and V_a, V_w are the volumes of air and water respectively. Air is assumed to be distributed evenly throughout the flow in the above formulae, which have been derived for chutes having rectangular cross sections. Both hypotheses are valid in the present contest. So the ratio between the two momentum equations becomes:

$$\frac{M_m}{M} = \frac{1-1.1\,C}{1-C} \qquad 0.2 \le C \le 0.85$$

The bore thrust is not remarkably affected by air–entrainment as long as air concentration in the toe is as high as, just to fix the ideas, 0.3. Of course the above reasoning is correct only if applied to steady state conditions but it seems reasonable to extend it in the first approximation to unsteady motion as well.

3. Analytical formulation of the problem

A clear water bore hitting upon a rigid, vertical, plane wall is considered herein. The surge is generated by the dam–break method and propagates over a dry bed. Such a problem can typically be formulated by assuming that at the initial time $t = 0$ the liquid mass meets the wall; at this moment, the wall location, the liquid domain and the flow field are assumed to be known. For $t > 0$ the flow field together with liquid actions on the wall have to be determined. As the very first consideration, it should be possible to evaluate the global quantities of interest with reasonable accuracy from rather simplified assumptions of the collision process, so that the closed form analytical solution of the phenomenon, if ever attainable, is not important. It is to be reminded that there seem to be no rigorous results of general value in non–linear unsteady problems with both a free streamline (a streamline which separates fluid in motion from fluid at rest) and a contact line. Some simplifying hypotheses must therefore be formulated.

The first one concerns the compressibility of the fluid that can be safely ignored in the present contest [Peregrine and Topliss, 1994]. Also, inertia forces are by far dominant as compared to surface tension, viscosity and gravity forces at almost any stage of the impact process, except for the last moments. The dynamic interaction of a structure with a liquid jet should be solved in principle as a unified hydro–elastic system; however, the elastic response of the structure would pose additional complexities in the computations and therefore the wall has been regarded as a rigid body in the present simulation. After all, calculated pressures would be on the safety side; in fact, a pressure overestimation of only $3\% \div 6\%$, as compared to the more realistic case of elastic wall, was claimed by Zhang et al. [1996].

Hence, assuming further that the flow is irrotational and time–dependent in a simply connected domain, bounded by impervious walls and a free streamline, it appears that the essential features involved in the collision process can be described by a simplified approach based on the potential flow theory. The velocity potential is basically the pres-

sure impulse capable of accelerating instantaneously the fluid at rest [Lamb, 1932]. The pressure–impulse concept can be applied when a body strikes a fluid or viceversa [Cooker and Peregrine, 1995].

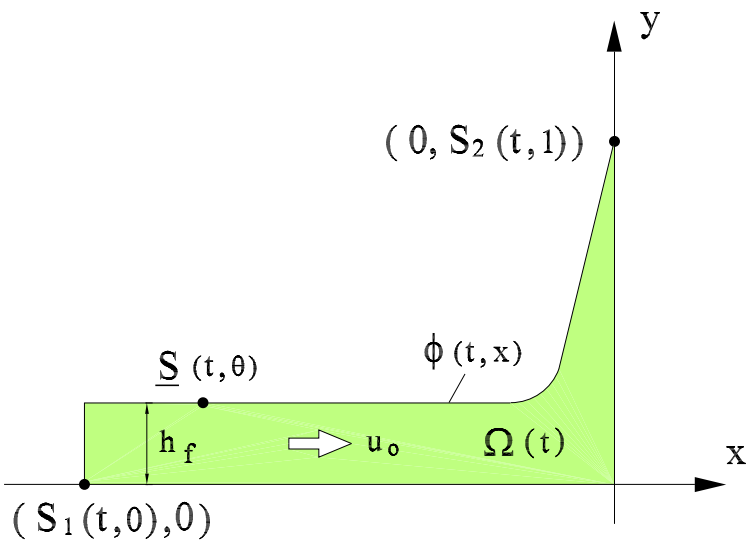

Figure 1: Sketch of the problem and notation

3.1. Domain of computation and boundary conditions

The computational liquid domain $\Omega(t)$ is assumed to be simply connected and time dependent (fig. 1). Its boundary, defined as $\partial\Omega(t)$, is composed by the free surface $\Gamma_s(t)$ and by the rigid, impermeable wall boundary $\Gamma_w(t)$:

$$\begin{aligned}
\partial\Omega(t) &= \Gamma_s(t) \cup \Gamma_w(t) \\
\Gamma_s(t) &= \{\mathbf{S}(t,\theta) \mid 0 \le \theta \le 1\} \\
\Gamma_w(t) &= \{(x,0) \mid S_1(t,0) \le x \le 0\} \cup \{(0,y) \mid 0 \le y \le S_2(t,1)\}
\end{aligned}$$

where $\mathbf{S}(t,\theta)$, the components of which are $S_1(t,\theta)$ and $S_2(t,\theta)$, is the parametric form of the *moving* free streamline; θ is a parameter running in the closed interval $[0,1]$.

Recalling the considerations developed in the above paragraph, the velocity potential $\Phi = \Phi(t,\mathbf{x})$ satisfies Laplace's equation in the domain $\Omega(t)$ at any time t, supplemented by suitable boundary conditions:

$$\begin{cases} \nabla^2\Phi(t,\mathbf{x}) = 0, & \mathbf{x} \text{ in } \Omega(t) \text{ and } t \geq 0 \\ \nabla\Phi(t,\mathbf{x}) \cdot \mathbf{n} = 0 & \mathbf{x} \text{ on } \Gamma_w(t) \text{ and } t \geq 0 \\ \Phi(t,\mathbf{S}(t,\theta)) = \phi(t,\theta) & \theta \text{ in } [0,1] \text{ and } t \geq 0 \end{cases} \tag{3.1}$$

where $\nabla^2 = \frac{\partial^2}{\partial x^2} + \frac{\partial^2}{\partial y^2}$, $\mathbf{n}$ is the outward normal to the boundary and $\phi(t,\theta)$ stands for the potential function along the free surface. The velocity vector $\mathbf{V} = (u,v)$ has horizontal $u = u(t,\mathbf{x})$ and vertical $v = v(t,\mathbf{x})$ components of velocity, apparently the derivatives of the potential:

$$u(t,\mathbf{x}) = \frac{\partial\Phi}{\partial x}(t,\mathbf{x}), \qquad v(t,\mathbf{x}) = \frac{\partial\Phi}{\partial y}(t,\mathbf{x})$$

3.2. Free surface dynamic conditions

The parametric equations of the free surface evolution can be derived knowing the velocity field $\mathbf{V}_s$ on $\Gamma_s(t)$:

$$\frac{\partial\mathbf{S}}{\partial t}(t,\theta) = \mathbf{V}_s(t,\theta) \tag{3.2}$$

The Euler's equation can be manipulated to obtain the dynamic boundary condition on the inviscid free surface. By taking advantage of the flow irrotationality and by inserting the potential function in the Euler's equation, integrating spatially and imposing that the pressure acting on the free surface must equal the external ambient pressure (which is taken as the reference pressure, assumed to be zero), the boundary condition on the free

streamline is obtained:

$$\frac{\partial \phi}{\partial t}(t,\theta) = \frac{1}{2}\left\|\mathbf{V}_s(t,\theta)\right\|^2 \tag{3.3}$$

where $\|\mathbf{V}_s\| = \sqrt{\mathbf{V}_s \cdot \mathbf{V}_s}$ is the familiar Euclidean norm. Condition (3.3) is known as the non–linear dynamic condition on the free surface or also as Bernoulli's equation. Equation (3.1) is used to compute $\mathbf{V}_s(t,\theta)$.

3.3. Initial condition

At the initial time $t = 0$ the surge strikes the wall and starts to move upward; the free surface is therefore deflected up to a distance of influence L_o.

The actual initial condition is not known from the physical experiments. Instead, only the toe bore velocity was measured, apparently a rough estimate of the bulk velocity. Nonetheless it was decided to assign the same velocity field $(u_o, 0)$ for all $\mathbf{x} \in \Omega(0)$ so as to provide a test of the numerical scheme. As a result, the initial domain, i.e. the approaching bore, is a rectangle, since an inviscid liquid jet must be straight whenever the speed is the same on both boundaries [Milne-Thompson, 1968]. This is a good approximation since the physical toe was seen by video camera observations to be mildly elongated along its direction of propagation. The initial condition provides the starting value of the potential in the domain $\Omega(t)$:

$$\Phi(0,\mathbf{x}) = \Phi_0(\mathbf{x}), \qquad \mathbf{x} \text{ in } \Omega(0)$$

and on the free surface:

$$\begin{aligned} \mathbf{S}(0,\theta) &= \mathbf{S}_0(\theta), && \theta \text{ in } [0,1] \\ \phi(0,\theta) &= \Phi_0(\mathbf{S}_0(\theta)), && \theta \text{ in } [0,1] \end{aligned}$$

where the potential of the initial uniform flow field is $\Phi_0(\mathbf{x}) = u_o x$.

4. The solution algorithm

4.1. The spatial discretization of the domain

The domain of definition of θ is divided into $N-1$ equal intervals:

$$0 = \theta_1 < \theta_2 < \cdots < \theta_N = 1$$

The whole computational domain $\Omega(t)$ is approximated by $\Omega_h(t)$, whose closed boundary $\partial\Omega_h(t)$ is piecewise linear. $\Omega_h(t)$ is then triangulated by any mesh generator. In the present work, the mesh generator code TRIANGLE (see Acknowledgements) has been used. TRIANGLE is based on a frontal method and supports the area-constraint option. The code generates Delaunay unstructured triangulations, giving nodal coordinates and topological relations.

The nodes of the mesh belonging to the free surface are numbered from 1 to N, while the remaining ones are numbered from $N+1$ to K. N is set at the beginning of the computation, while $K(n)$ is a number that is controlled by the partition generated at the $n-$th time step.

The set of the generated triangles is assumed regular [Ciarlet, 1980, Zlamal, 1968]; T_{ijk} is the generic triangle whose vertices are i, j and k; $\mathcal{C} = \{C_i\}_{i=1}^{K}$ is the set of covolumes (see figure 2) related to the vertices of Ω_h.

Some definitions are also useful for the sake of conciseness:

$$\mathbf{S}_i(t) = \mathbf{S}(t, \theta_i) \qquad \phi_i(t) = \phi(t, \theta_i) \qquad \mathbf{V}_i(t) = \mathbf{V}_s(t, \theta_i)$$

Evaluating (3.2) and (3.3) on θ_i, the following discrete formulation for the free surface

location and potential is obtained:

$$\begin{aligned} \frac{\partial \mathbf{S}_i}{\partial t} &= \mathbf{V}_i\,, & i &= 1,2,\ldots,N \\ \frac{\partial \phi_i}{\partial t} &= \frac{1}{2}\left\|\mathbf{V}_i\right\|^2\,, & i &= 1,2,\ldots,N \end{aligned}$$

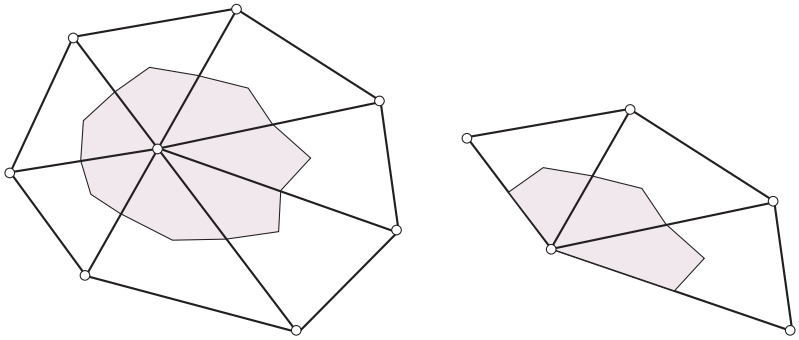

Figure 2: Internal covolume and boundary covolume

4.2. Time advancing

It is assumed that the free surface location $\mathbf{S}_i^n$ and the potential along the free surface ϕ_i^n are known at the time t^n. The time marching is performed by the two stage second-order Runge–Kutta scheme [Heun, 1900]:

4.2.1. Predictor step

- Estimating the free surface at time t^{n+1}:

$$\mathbf{S}_i^{n+*} = \mathbf{S}_i^n + \Delta t\,\mathbf{V}_i^n, \qquad i = 1,2,\ldots,N$$

- Estimating the surface potential at time t^{n+1}:

$$\phi_i^{n+*} = \phi_i^n + \frac{\Delta t}{2}\left\|\mathbf{V}_i^n\right\|^2, \qquad i = 1,2,\ldots,N$$

4.2.2. Corrector step

- Correcting the free surface at time t^{n+1}:

$$\mathbf{S}_i^{n+1} = \mathbf{S}_i^n + \frac{\Delta t}{2}\left(\mathbf{V}_i^n + \mathbf{V}_i^{n+*}\right), \qquad i = 1, 2, \ldots, N$$

- Correcting the surface potential at time t^{n+1}:

$$\phi_i^{n+1} = \phi_i^n + \frac{\Delta t}{4}\left(\left\|\mathbf{V}_i^n\right\|^2 + \left\|\mathbf{V}_i^{n+*}\right\|^2\right), \qquad i = 1, 2, \ldots, N$$

4.3. The computation of $\mathbf{V}_i^n$ *and* $\mathbf{V}_i^{n+*}$

The free surface nodal velocities $\mathbf{V}_i^n$ are estimated by solving numerically the problem (3.1). Likewise for $\mathbf{V}_i^{n+*}$. Problem (3.1) is solved by a Finite Volume Element (FVE) scheme after the meshing of the domain $\Omega_h(t)$. The meshing of $\Omega_h(t^n)$ is performed by TRIANGLE, while the meshing of $\Omega_h(t^{n+*})$ is done by stretching the whole mesh computed at the time t^n.

4.4. Discrete Primitive Formulation

The Boundary Element Method (BEM) could have been implemented: however, owing to the expected extension of the present model involving a heterogeneous computational domain and more realistic initial conditions for the velocity field, the BEM is clearly not suitable. For generality's sake, therefore, a FVE scheme [Cai et al., 1991, Huang and Xi, 1998] has been implemented to solve problem (3.1).

The mesh manager useful to construct the FVE approximation has been performed by means of P2MESH [Bertolazzi and Manzini, 1999], which is a free software package conceived for the fast development of Finite Volume and Finite Element codes on 2–D *unstructured* mesh.

FVE schemes are based on a primitive formulation of problem (3.1). Integrating (3.1) over covolume C_i and by taking advantage of the Gauss–Green formula together with

Neumann boundary conditions at time $t = t^n$:

$$\int_{\partial C_i \setminus \partial\Omega} \nabla\Phi(t^n, \mathbf{x}) \cdot \mathbf{n} = 0, \qquad i = N+1, 2, \ldots, K \tag{4.1}$$

the discrete formulation is obtained approximating Φ by means of the $\mathbb{P}^1$ finite element polynomials:

$$\Phi(t^n, \mathbf{x}) \approx \sum_{i=1}^{N} \phi_i^n \Psi_i^n(\mathbf{x}) + \sum_{i=N+1}^{K} \Phi_i^n \Psi_i^n(\mathbf{x})$$

Combining with (4.1):

$$\begin{aligned} &\sum_{j=N+1}^{K} \Phi_j^n \int_{\partial C_i \setminus \partial\Omega} \nabla\Psi_j^n(\mathbf{x}) \cdot \mathbf{n} \; + \\ &\sum_{j=N+1}^{K} \phi_j^n \int_{\partial C_i \setminus \partial\Omega} \nabla\Psi_j^n(\mathbf{x}) \cdot \mathbf{n} \; = \; 0, \qquad i = N+1, 2, \ldots, K \end{aligned} \tag{4.2}$$

The result of (4.2) is a linear system of $K - N$ equations in $K - N$ unknowns; owing to the constancy of $\nabla\Psi_j^n(\mathbf{x})$ over triangles, the system can be written as:

$$\sum_{j=N+1}^{K} A_{ij}^n \Phi_j^n = -\sum_{j=1}^{N} A_{ij}^n \phi_j^n, \qquad i = N+1, 2, \ldots, K$$

where:

$$A_{ij}^n = \sum_{T_{ijk} \in \mathcal{T}} \nabla\Psi_{ijk}^n \cdot \int_{\partial C_i \cap T_{ijk}} \mathbf{n}. \tag{4.3}$$

and $\nabla\Psi_{ijk}$ is the value of the gradient of $\Psi_i(\mathbf{x})$ over T_{ijk}:

$$\Psi_i(\mathbf{x}) = \frac{(\mathbf{x} - \mathbf{x}_j)\mathbf{R}(\mathbf{x}_j - \mathbf{x}_k)}{2\,|\,T_{ijk}|}, \qquad \nabla\Psi_{ijk} = \frac{\mathbf{R}(\mathbf{x}_j - \mathbf{x}_k)}{2\,|\,T_{ijk}|}, \qquad \mathbf{R} = \begin{pmatrix} 0 & 1 \\ -1 & 0 \end{pmatrix}$$

The evaluation of the integral in (4.3) yields (fig. 3):

$$\int_{\partial C_i \cap T_{ijk}} \mathbf{n} = \frac{1}{2}\mathbf{R}(\mathbf{x}_k - \mathbf{x}_j),$$

Then, recalling that $\mathbf{R}^T\mathbf{R} = \mathbf{I}$, it is eventually obtained:

$$\nabla\Psi^n_{ijk} \cdot \int_{\partial C_i \cap T_{ijk}} \mathbf{n} = \frac{(\mathbf{x}_k - \mathbf{x}_i) \cdot (\mathbf{x}_j - \mathbf{x}_k)}{4\,|T_{ijk}|}$$

It is observed that the resulting system matrix is the same as the $\mathbb{P}^1$ finite element matrix [Hackbusch, 1989, Huang and Xi, 1998].

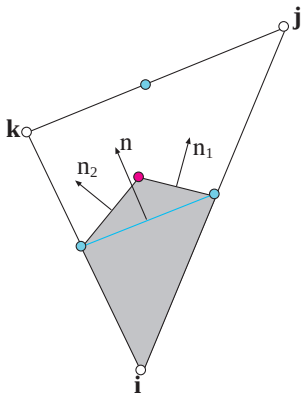

Figure 3: Sketch of the evaluation of the integral in equation (4.3)

5. Numerical simulations

The laboratory experimental impact chosen to test the numerical model is the clear water bore detailed by Scotton [1996] and by Trivellato and Scotton [2001].

The quantities that have been assumed as the initial conditions of the numerical model are $u_o = 2.77\,\mathrm{m/s}$ (toe velocity) and $h_f = 0.04\,\mathrm{m}$ (toe depth). Both quantities are the picture of an instant of time and are not supposed to be the representative ones of a highly

unsteady phenomenon. Instantaneous measurements of toe velocities do embody turbulent streamwise fluctuations, which are believed to be as high as $\pm 10\%$ of the average velocity. In addition, assigning the initial velocity $(u_o, 0)$ to *all* of the nodes of the domain is no doubt a rough approximation. Hence nothing more than a qualitative agreement should be expected from the numerical comparison. Air entrainment and gravity have both been neglected in the numerical computations.

The upstream length of the rectangular liquid domain was set $3\,\mathrm{m}$. By trial and error a convenient temporal step was found to be $2.5 \cdot 10^{-5}\,\mathrm{s}$. The typical number of generated triangles was 1000. The typical CPU time for a complete simulation, involving $2 \cdot 10^4$ time steps, was half an hour in a Digital DEC 1000A/500 machine.

5.1. Grid and free surface.

The highly unsteady evolution of the free surface turned out to be definitely the most difficult problem to manage. The grid is depicted in Fig. 4 at the times 0.1, 0.2 and $0.3\,\mathrm{s}$, where only about 40% of the computed region is shown.

The model predicts the moving free surface while verifying closely the mass conservation. It has to be pointed out that the accurate modeling of the free surface is not important as far as the calculation of the wall pressure is concerned; in fact it was observed in the present numerical simulation that different schematizations of the impacting liquid shape affect the wall pressure evolution by a small amount. Cooker and Peregrine [1995] found a relative insensitivity to the shape of the incident free boundary, which is a result of relevant value in practical circumstances; this implies that even simple schematizations of the free surface can be effective, since wall pressure is not much affected both by the jet shape and by the liquid body further away from the rigid surface. Roughly at the time $0.2\,\mathrm{s}$ a sort of sawtooth instability starts to develop on the free streamline, but remains limited in size and does not increase. At the end of the $0.5\,\mathrm{s}$ simulation the code is still stable The sawtooth instability is not new in literature: since Longuet-Higgins and Stewart [1960] it has been detected in other instances by many investigators. As a matter of fact, computational

instabilities are known to be inherent in the inviscid, incompressible, free surface model. Temporal discretization has no effect on the stability of the problem. Instead, spatial discretization of the domain promotes instabilities whenever the mesh is not symmetric, due to the dispersive nature of the resulting discrete operator. Techniques have been devised to enforce stability by inhibiting the growth of the sawtooth pattern: removal of high modes, smoothing techniques and addition of a diffusive term to the kinematic boundary condition are in this contest among the most popular procedures, a review of which is found in Robertson and Sherwin [1999]. The treatment of the numerical instabilities of the free surface has not been pursued in this work, as the experimental free surface profile shows a huge air entrainment, phenomenon which has not been accounted for in the numerical simulation (Fig. 5). The computed free streamline evolves towards the steady state solution (Fig. 6).

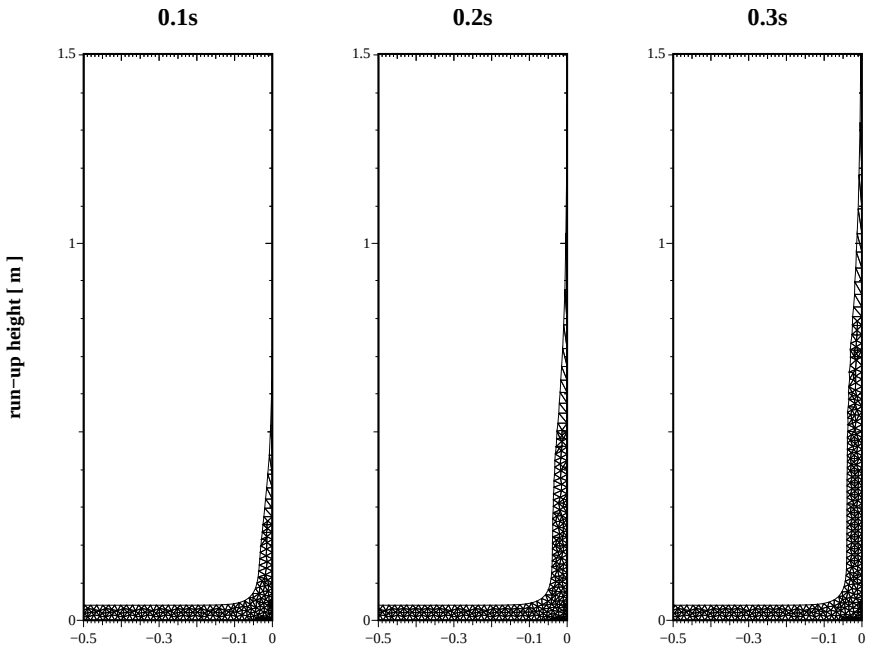

Figure 4: grids at 0.1, 0.2 and 0.3 s (flow is from left to right)

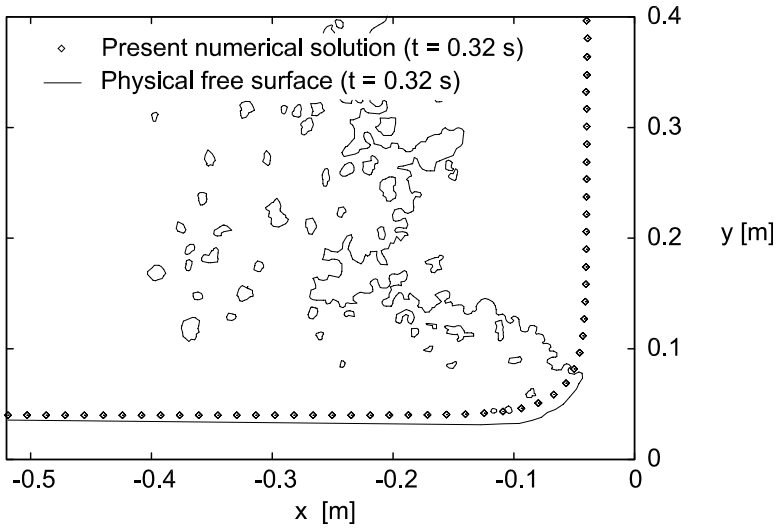

Figure 5: Measured and computed free surface (flow is from left to right)

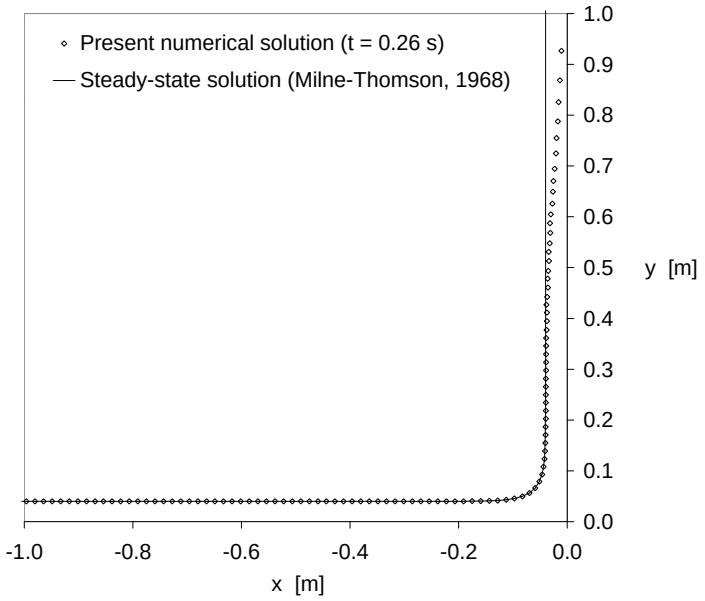

Figure 6: Evolution towards the steady state (flow is from left to right)

5.2. The wall pressure

The temporal evolution of wall pressure in two gauges is presented in Fig. 7. The gauges are located at a distance of 0.5 and 6.5 cm along the vertical wall, starting from the bottom floor. Since the gravity force has been neglected in the computation, the wall pressure does not include the hydrostatic component. The tiny oscillations of the pressure diagram are not physical: they are due to the nodes of the moving mesh (which is rebuilt at any time step) passing through the gauge's location. The time history evolves towards the steady state roughly in a tenth of a second. The pressure is highest in the lower region, clearly the stagnation region. The numerically computed pressure cannot in principle be compared straightforwardly to the physically measured pressure due to the dramatic difference of the initial conditions in the physical and numerical tests; anyway, the estimate given by the numerical simulation for the wall pressure is approximately twice the measured pressure for the lowest gauge, while the experimental pressure is fairly well predicted in the 6.5 cm gauge.

The pressure on the wall is illustrated in Fig. 8. There is basically no difference between the wall pressure from 0.1 to 0.3 s. The pressure is most effective in the lower region, clearly the stagnation region. The distance of influence L_o is the wall distance, computed from the bottom, where the pressure distribution along the wall normal is hydrostatic, as it can be readily obtained by the Euler's second equation written in streamline coordinates; as a matter of fact, the free streamline is parallel to the wall from L_o upward, at least after a time interval – normally tiny indeed – elapsed from the beginning of the impact. In the experimental database [Trivellato and Scotton, 2001], L_o/h_f ranges typically from 2.5 through 7 and in the present case study $L_o/h_f = 2.9$; it can be seen in Fig. 8 that the pressure is close to zero at $L_o/h_f \sim 4$. Considering further the approximation involved in the physical measurement of L_o, this result compares favourably with the solution pertaining to the steady impact [Milne-Thompson, 1968], where the distance of positive pressures is four times the length scale h_f. A *pseudo* steady state is presented in Fig. 9 at $t = 0.3$ s, where the symmetry about the bisetrix of the axes has been clearly

reached by the numerical liquid jet. This symmetry feature is also embodied by the steady state analytical solution [Milne-Thompson, 1968, Peng and Parker, 1997]. The computed wall pressure evolves towards the steady state (Fig. 10).

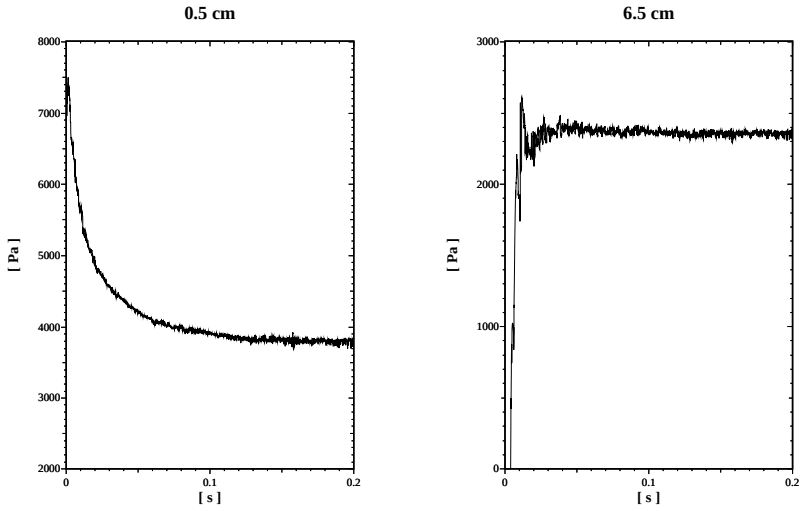

Figure 7: Pressure time history at two wall gauges (located at 0.5 cm and 6.5 cm

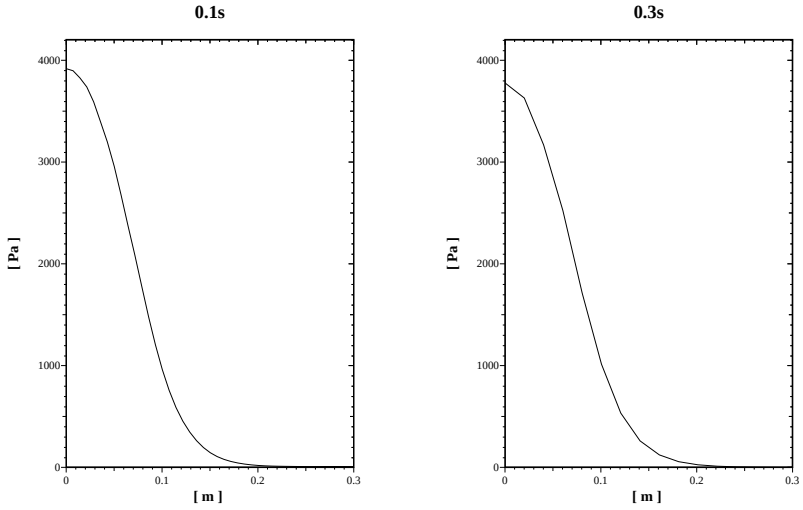

Figure 8: Wall pressure at 0.1 and 0.3 s

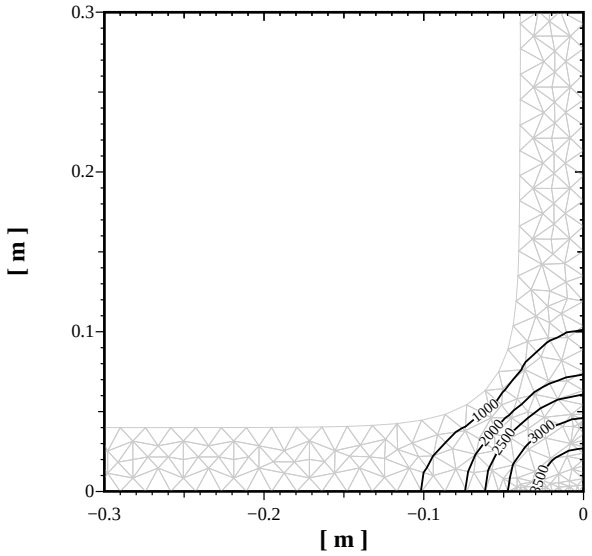

Figure 9: Isobars at 0.3 s (flow is from left to right; pressure in Pascal)

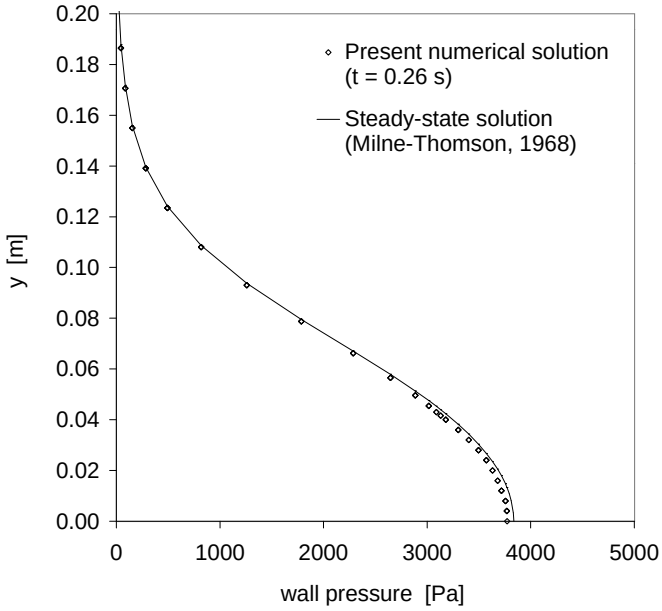

Figure 10: Wall pressure evolves to the steady state

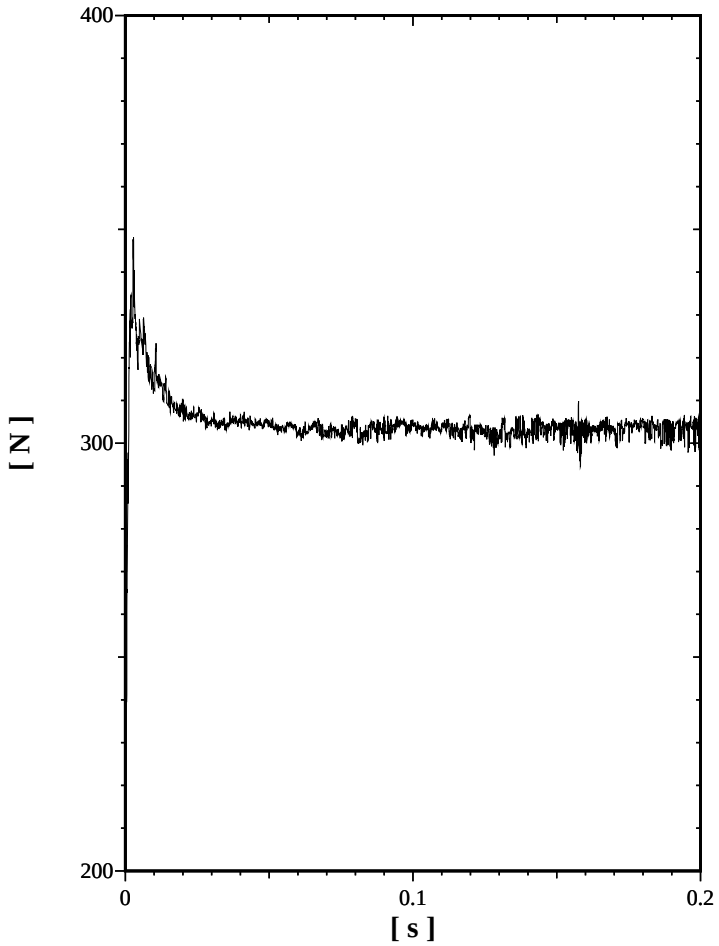

Figure 11: Temporal evolution of the wall force

5.3. The wall force

The knowledge of the wall force is normally a more relevant quantity for design than the maximum impact pressure. The force acting on the rigid surface is obtained by integrating the pressure diagrams and its temporal evolution is illustrated in Fig. 11. The maximum force occurs at the time $T_r = 0.003\,\mathrm{s}$. As far as the sea wave impact is concerned, it is known that T_r is of the order of milliseconds or so [Peregrine and Topliss, 1994]. The

numerical model overestimates the maximum measured force by a factor of 1.4. A check to the wall force numerical prediction is provided by the theoretical horizontal steady thrust of the clear water bore $M = \rho Q u_o = \rho u_o^2 h_f$, that is equal to $307\ N$, a result in close agreement with the asymptotic value of Fig. 11.

6. Conclusions

The numerical modeling of an inviscid dam–break surge as it advances over a dry bed and strikes a rigid wall is new in literature. The knowledge of the dynamic loading due to the bore impact is of interest to the civil engineer in a number of practical instances. In the present study the problem has been tackled in the framework of the potential theory. The flow is assumed to be irrotational and time–dependent in a simply connected domain, bounded by impervious walls and a free streamline. In comparison with inertial effects, the influence of viscosity, surface tension and gravity is supposedly small and has been neglected. The liquid density is constant. Even if reduced to the potential theory level, the problem still poses significant challenges due to the highly non–linear nature of the free surface boundary conditions. While the present numerical model needs to be thoroughly corroborated by more realistic initial conditions, however it seems capable of reproducing with sufficient accuracy the non–linear impact of a dam–break surge.

There seem there are reasons to believe that, at least as far as the wall force and bending moment are concerned, meaningful predictions for the prototype can be obtained not only from laboratory tests but also from numerical simulations, considering also the order of magnitude of the errors involved in the experimental laboratory measurements.

The animation of the impact, based on the present numerical simulation, can be watched and downloaded at the following URL :

`http://www.ing.unitn.it/~bertolaz`

References

A. Armanini and P. Scotton. On the dynamic impact of a debris flow on structures. In *Proceedings, B–6–4, XXV IAHR Congress*, pages 203–210, Tokyo, Japan, 1993.

A. Armanini and F. Trivellato. Physical modelling of debris flow. In *Proceedings, 22th National Congress of Hydraulics and Hydraulic Structures*, pages 235–247, Cosenza, Italy (in Italian), 1990.

R.F. Beck. *Fully non linear water wave computations using a desingularized Euler–Lagrange time–domain approach, in "Non linear water wave interaction"*, chapter 1. WIT Press, Ashurst, Great Britain, 1999.

S. Beltaos and N. Rajaratnam. Impinging circular turbulent jets. *ASCE, Journal of Hydraulic Division*, 100:1313–1328, 1974.

E. Bertolazzi and G. Manzini. The P2MESH Home Page, 1999. `http://www.ing.unitn.it/~bertolaz/bery.p2mesh.shtml`.

Z. Q. Cai, J. Mandel, and S. McCormick. The finite volume element method for diffusion equations on general triangulations. *SIAM J. Numer. Anal.*, 28(2):392–402, 1991. ISSN 0036-1429.

H. Chanson. Self aerated flows on chutes and spillways. *Journal of Hydraulic Engineering*, 119(2):220–243, 1993.

P. G. Ciarlet. *The finite element method for elliptic problems*. North-Holland Publishing Company, Amsterdam, Holland, 1980.

M. J. Cooker and D. H. Peregrine. Pressure impulse theory for liquid impact problems. *Journal of Fluid Mechanics*, 297:193–214, 1995.

R. H. Cross. Tsunamis surge forces. *Journal of the Waterways and Harbor Division, ASCE*, 93 (WW4):201–231, 1967.

E. Cumberbatch. The impact of a water wedge on a wall. *Journal of Fluid Mechanics*, 7: 353–374, 1960.

J.W. Dold and D.H. Peregrine. An efficient boundary–integral method for steep unsteady water waves. In *Proceedings, in Numerical Methods for Fluid Dynamics*, pages 671–679, Editions Morton K.W.&Baines, Oxford University Press, Great Britain, 1986.

A. Führböter. Model and prototype tests for wave impact and run–up on a uniform 1:4 slope. *Coastal Engineering*, 10:49–84, 1986.

Y. Goda. Random seas and the design of maritime structures. Technical report, University of Tokyo Press, Tokyo, Japan, 1985.

W. Hackbusch. On first and second order box schemes. *Computing*, 41(4):277–296, 1989. ISSN 0010-485X.

K. Heun. Methode zur approximativen integration der differentialgleichungen einer unabhängigen variablen. *Z. Math. Phys.*, 45, 1900.

J. Huang and S. Xi. On the finite volume element method for general self-adjoint elliptic problems. *SIAM J. Numer. Anal.*, 35(5):1762–1774, 1998. ISSN 1095-7170.

M.S. Kirkgöz. Shock pressure of breaking waves on vertical walls. *Journal of Waterways, Port, Ocean Engineering Division, ASCE*, 108:81–95, 1982.

A. A. Korobkin and D. H. Peregrine. The energy distribution resulting from an impact on a floating body. *Journal of Fluid Mechanics*, 417:157–181, 2000.

A. A. Korobkin and V. V. Pukhnachov. *Initial stage of water impact*, chapter 20, pages 159–185. Annual review of fluid mechanics, 1988.

H. Lamb. *Hydrodynamics, 6th Edition*. Cambridge University Press, Great Britain, 1932.

M. S. Longuet-Higgins and R. W. Stewart. Changes in the form of short gravity waves on long waves and tidal currents. *Journal of Fluid Mechanics*, 8:565–583, 1960.

J. W. Miles. Impulsive motion of a flat plate. *Quarterly Journal of Mechanics and Applied Mathematics*, VI Pt. 2:129–140, 1953.

L. M. Milne-Thompson. *Theoretical Hydrodynamics, 5th Edition*. MacMillan, New York, 1968.

P. K. Mohapatra, S.M. Bhallamudi, and V. Eswaran. Numerical simulation of impact of bores against inclined walls. *Journal of Hydraulic Engineering*, 126(12):942–945, 2000.

S. Okubo, H. Ikeya, Y. Ishikawa, and T. Yamada. *Development of new methods for countermeasures against debris flows, Lecture notes in Earth Sciences, n. 64*, chapter 3. Springer–Verlag, Berlin, 1997.

W. Peng and D. F. Parker. An ideal fluid jet impinging on an uneven wall. *Journal of Fluid Mechanics*, 333:231–255, 1997.

D. H. Peregrine and L. Thais. The effect of entrained air in violent water wave impacts. *Journal of Fluid Mechanics*, 325:377–397, 1996.

D. H. Peregrine and M. E. Topliss. The impact of water waves upon a wall. In *Proceedings of the IUTAM/ISIMM Symposium on Structure and Dynamics of Nonlinear Waves in Fluids, 17–20 August*, pages 83–98, 1994.

D. J. Phares, G. T. Smedley, and R. C. Flagan. The wall shear stress produced by the normal impingement of a jet on a flat surface. *Journal of Fluid Mechanics*, 418:351–375, 2000.

J. D. Ramsden and F. Raichlen. Forces on vertical wall caused by incident bores. *Journal of Waterway, Port, Coastal and Ocean Engineering*, 116(5):592–613, 1990.

N.S.G. Rao and H. Kobus. *Characteristics of self–aerated free–surface flows*. Erich Schmidt Verlag, Berlin, Germany, 1973.

I. Robertson and S. Sherwin. Free surface flow simulation using hp/spectral elements. *Journal of Computational Physics*, 155:26–53, 1999.

P. Scotton. Dynamic impact of debris flow : experimental study. Technical report, IDR2, Department of Civil and Environmental Engineering, University of Trento, Italy, 1996.

P. Scotton and F. Trivellato. Dynamic pressure on check–dam due to debris flow collision. In *Proceedings, Twelfth Australasian Fluid Mechanics Conference*, Sydney, Australia, 1995a.

P. Scotton and F. Trivellato. Vulnerability of check–dams. In *Proceedings, 7th Congress*

on Seismic Engineering, Siena, Italy (in Italian), 1995b.

S. Shin and W. I. Lee. Finite element analysis of incompressible viscous flow with moving free surface by selective volume of fluid method. *International Journal of Heat and Fluid Flow*, 21:197–206, 2000.

F. Trivellato and P. Scotton. Bore impact upon a wall (experimental database). Technical report, Department of Civil and Environmental Engineering, University of Trento, Italy, 2001.

R. Weber and J. Hureau. Impact of an ideal fluid jet on a curved wall: the inverse problem. *European Journal of Mechanics, B/Fluids*, 18:283–294, 1999.

H. W. Westergaard. Water pressures on dams due to horizontal earthquakes effects. *Transactions ASCE*, 98:418–433, 1933.

A. F. Whillock. Measurements of forces resulting from normal and oblique wave approaches to small scale sea walls. *Coastal Engineering*, 11:297–308, 1987.

D. J. Wood and D. H. Peregrine. Wave impact on a wall using pressure–impulse theory. part ii: Porous berm. *Journal of Waterway, Port, Coastal and Ocean Engineering*, 126(4): 191–195, 2000.

D. J. Wood, D. H. Peregrine, and T. Bruce. Wave impact on a wall using pressure–impulse theory. part i: Trapped air. *Journal of Waterway, Port, Coastal and Ocean Engineering*, 126(4):182–190, 2000.

S. Zhang, D. K. P. Yue, and K. Tanizawa. Simulation of plunging wave impact on a vertical wall. *Journal of Fluid Mechanics*, 327:221–254, 1996.

M. Zlamal. On the finite element method. *Numerische Mathematik*, 12:394–409, 1968. ISSN 0029-599X (print), 0945-3245.

Acknowledgements

The unstructured Delaunay grids were generated by the mesh generator TRIANGLE, a code implemented by Shewchuck, see the *URL*: `http://almond.srv.cs.cmu.edu/afs/cs/project/quake/public/www/triangle.html`.

The authors are grateful to Dr. Luca Formaggia, EPFL, Lausanne (Ch); Dr. Giammarco Manzini, IAR-CNR, Pavia (I); Dr. A. Marion, IMAGE, Padua (I) and Prof. Walter C. Mih, Washington State University (Usa) for the suggestions offered in reviewing the draft of the paper.